Advances in Bioresearch
Adv. Biores., Vol 13 (3) May 2022: 161-173
©2022 Society of Education, India
Print ISSN 0976-4585; Online ISSN 2277-1573
Journal's URL:http://www.soeagra.com/abr.html
CODEN: ABRDC3
DOI: 10.15515/abr.0976-4585.13.3.161173

Advances in Bioresearch

ORIGINAL ARTICLE

Consistency Measurement for Different-Scale Satellite Data Sets Applied on Vegetation Assessment: Case Study Al-Ahsa Province, Saudi Arabia

[1]**Abdelrahim Salih,** [2, 3*]**Abdalhaleem A. Hassaballa,** [1]**Yasin Elhadary**
[1]Department of Geography, Al-Imam Muhammad Ibn Saud Islamic University, Al-Hofuf, Al-Ahsa, Saudi Arabia.
[2]Department of Environment and Agricultural Natural Resources, Faculty of Agriculture and Food Sciences, King Faisal University, Al-Hofuf, Al-Ahsa, Saudi Arabia.
[3]Department of Agricultural and Biological Engineering, Faculty of Engineering, University of Khartoum, Sudan.
*Corresponding Author's Email: ahassaballa@kfu.edu.sa

ABSTRACT
The variability in satellite's spectral and spatial resolutions has become a critical issue in the application of remotely sensed data to vegetation monitoring and assessment. This study aimed to examine the consistency between three spatial data sets having a synchronous-imaging time with different spatial resolutions, working on vegetation indices (VIs) applied over a date palms region in Saudi Arabia. A point-based correlation was applied at sub-pixel levels, where Landsat (30 m and pan-sharpened 15 m) and Sentinel-2A (10 m) were applied. The extracted VIs (the normalized difference vegetation index (NDVI) and soil-adjusted vegetation index (SAVI)) pixels were vectorized into points, considering their identical locations in the other sensor's maps, then were correlated. The result statistics showed noticeable differences in the VIs, exhibiting the least variability between the sensors for SAVI. However, NDVI was slightly varying. The extracted vegetation-area showed noticeable differences of 4.32% and 4.54% between Sentinel-2A and the original pixels of Landsat for SAVI and the NDVI, respectively, exhibiting the impact of spatial resolution in land use/cover mapping accuracy. The applied correlation revealed moderate agreements of SAVIs for Sentinel-2A against both Landsat sets, producing R^2 of 0.76, while Landsat's (original pixels) NDVI poorly correlated Sentinel's (R^2 = 0.50). The results were validated and were found to be weak, producing R^2 of 0.60 for both VIs, which was attributed to the differences in the spectral regions and crop status. The study findings confirm the suitability of using SAVI in areas dominated by palm trees.
Keywords; *Vegetation monitoring, sub-pixel analysis, Landsat OLI, Sentinel-2A MSI*

Received 22.03.2022 Revised 16.04.2022 Accepted 18.05.2022

How to cite this article:
A Salih, A A. Hassaballa, Y Elhadary. Consistency Measurement for Different-Scale Satellite Data Sets Applied on Vegetation Assessment: Case Study Al-Ahsa Province, Saudi Arabia. Adv. Biores. Vol 13 [3] May 2022. 161-173

INTRODUCTION

Vegetation indices (VIs) have received much attention previously and generated considerable recent research interest owing to their simplicity and applicability in different fields of science. VIs have been used by researchers since the 1960s [1] to examine and monitor vegetation cover using remotely sensed imagery from different sensors, with different spectral and spatial resolutions. VIs obtained from satellite imagery have been extensively used in determining vegetation biophysical variability and characteristics [1, 2], and have been investigated as potential sources of information in different hydrological, topographical, and environmental models [3]. However, previous studies have shown differences in VIs (e.g., response and continuity) derived from numerous remote sensor systems even for similar objects owing to the differences in various specifications of the sensors [2, 4]. These differences have become a critical issue in the application of remotely sensed data in vegetation monitoring and assessment [2]. For example, She *et al*. [2] found that the operational land imagery (OLI), Landsat, largely inherits the band-pass characteristics of the enhanced thematic mapper (ETM+) by incorporating a normalized difference

VI (NDVI), a soil-adjusted VI (SAVI), and an enhanced VI (EVI). More recently, Zhang et al. [5] established a relationship between the Sentinel-2A multi-spectral instrument (MSI) and Landsat-8 OLI by applying an NDVI. They revealed that for three processing levels, the MSI and OLI data had a good agreement, as determined by the coefficient of determination ($R^2 > 0.89$). Finally, Song and Veroustraete [6] found good linearity between the vegetation ten-day composite (VGT-S10) NDVI data obtained with a 1 × 1 km spatial resolution and an advanced very-high-resolution radiometer (AVHRR) and the global inventory modelling mapping studies (GIMMS) NDVI data with an 8 × 8 km spatial resolution. These studies concluded that the correlation between these sensor systems depended partially on the vegetation cover density. However, most of the reviewed studies and others found in the literature revealed a good linearity between the different sensors' systems yielding VIs conducted over vegetation species other than date palms, while here in this study we focused on the consistency measurement of such systems applied over areas dominated by date palms, such as the Al-Ahsa oasis in Saudi Arabia. In this oasis, the existence of multiple surface features (e.g., urban, recreational sites, small farms) within the green class causes some type of technical inadaptability for medium-resolution satellites, such as the Landsat, to precisely assess the vegetation cover.

The Al-Ahsa oasis is one of the most valuable and significant agricultural resource in the Kingdom of Saudi Arabia. The oasis cultivated area is approximated as 7000 ha, where 92% of this area is comprised of date palm trees of 40 different varieties [7, 8]. The economic background of this region is strongly related to agriculture, so that broad agricultural activities are practiced, which include the cultivation of diverse crops. Owing to its natural prosperity and location in the middle of a collection of earliest civilization sites, it had a concrete role in establishing cultural and commercial bonds between the oasis citizens of the Kingdom of Saudi Arabia and other nations. This diversion in the concept of agricultural practice has transformed the agricultural-based nature of the oasis into a type of cultural landscape with a natural heritage, causing a severe invasion of non-vegetative features against the green cover. These new surface features, found in the form of urbanization components, were generated during the developmental stage from 1973 to 1994, which was associated with rapid population growth [9], which in turn increased the demand for housing. Consequently, the authorities broadened residential schemes with the establishment/enhancement of services (water, roads, electricity, and communication facilities). It is noteworthy that the citizens began establishing recreational places within and beneath palm canopies to satisfy the rising cultural and social demands.

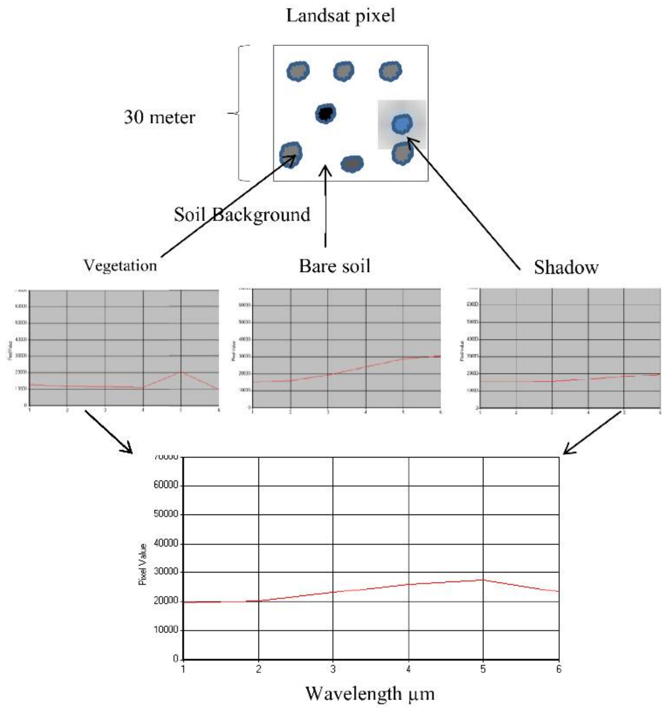

Figure1; A mixed spectra of Landsat TM (30 m) showing the multiple features within one pixel.

All the above mentioned activities have provided concrete reasons for diversifying the oasis vegetation cover to multiple surface features within the green class, causing some type of technical inadaptability for medium-resolution satellites, such as the Landsat series (30 m), to precisely assessing its vegetation cover. Instead, the use of a spectral response from the complete surface cover has become dominant. This concept of using a spectral mixture and its analysis for arid and semi-arid lands has been previously explained [10]. The spectra of the 30-m area of the Landsat Thematic Mapper sensor compiles a part of multiple features (Figure 1). Indeed, a process of sub-pixel discrimination for an area such as the Al-Ahsa oasis would enhance the entire analysis and resultant findings.

The overall aim of this study was to describe and examine the issues of reliability and consistency of SAVI and the NDVI of the Sentinel-2A MSI versus the original and pan-sharpened pixels of the Landsat-8 OLI datasets applied to an area dominated by date palm trees. Specifically, the objective of this study was to investigate the effect of the difference in the spatial and spectral resolutions of the above-mentioned satellite datasets on the SAVI and NDVI values over the study area. To confirm our results we used a uniform homogenous irrigated field within the study region as the validation plot.

MATERIAL AND METHODS

Study area

Administratively, the Kingdom of Saudi Arabia is divided into 13 regions (Emirates), with each region having its own provinces and centers. With an area of 672,522 km², the eastern region is considered as the largest region in the kingdom. Moreover, the region is also classified as the third region after Riyadh and Makkah in terms of population. In the 2010 census, the region counted 4.1 million inhabitants, representing approximately 15% of the Saudi total population. Besides the capital city of the region, Dammam, the region has several cities such as Al-Hofuf, Al-Jubail, Al-Khobar, and Al-Qatif. The eastern region itself has 12 provinces and 16 centers [11]. The study area mainly contained the Al-Ahsa province, which is one of the major parts of the region.

The Al-Ahsa province covers an area of approximately 534,000 km², representing 24% of the total area of the kingdom and 67% of the eastern region, with an estimated population of more than 1 million. The Al-Ahsa main cities (Hofuf and Mubarraz) are located in the northern part of the province, approximately 150 km south of the Dammam port and 320 km southeast of Riyadh (the capital city of the kingdom). These two major cities encompass an area of approximately 22,898 km². It is bordered by an eastern oasis in the north, a southern oasis in the south, the Arabian-American Oil Company (ARAMCO) in the west, and the Al-Ahsa airport in the southwest [12, 13].The study area lies within the Al-Ahsa province and covers an area of approximately 2268.72 km², extending between longitudes of 49°24'– 49°48' E and latitudes 25°24'– 25°36' N (Figure 2), with an approximate elevation of 130 to 160 m above sea level [14]. The area is oriented as a long part stretching for 25 km in the north–south direction and a short part of 18 km in the east–west direction.

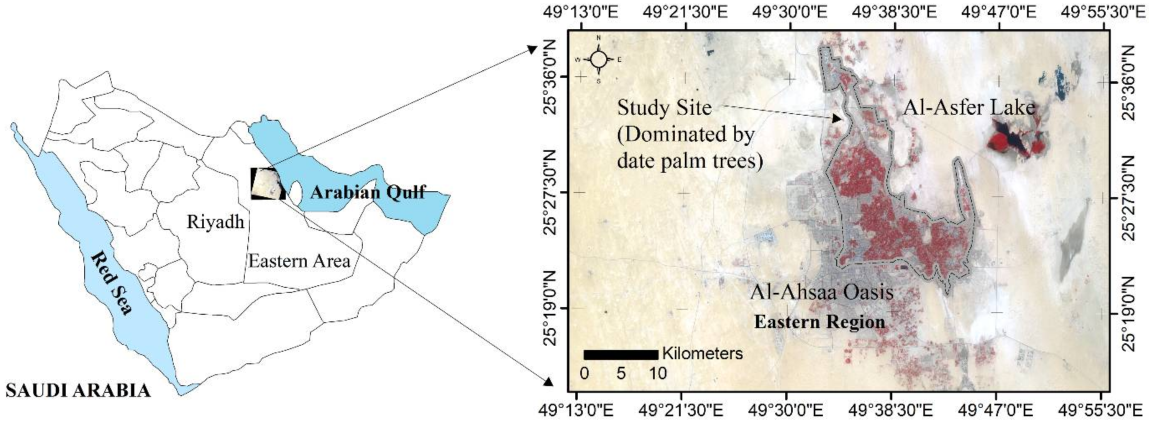

Figure2; Location of the study area within the eastern region of Saudi Arabia, Satellite image is from Landsat-8 (OLI) using channels 3,4,5 RGB.

Based on a population survey conducted in 2017, the oasis population was estimated as 800,000, of which 78% were living in urban areas and 22% in rural areas and villages [15]. According to the data from a recent study by Abdelatti et al. [9], the population of the Al-Ahsa oasis rose from 445,000 in 1992 to 768,000 in 2016. The number of housing units in the province in 2017 was 149,905, representing 24.2% (618,628) of the total units of the eastern region [11]. In 1994, nearly 4.4% of the buildings were still mud and wood; in 2014, 70% of the houses were converted into concrete and cement structures, 25% made of bricks and 5% of stone, with no mud and wood houses [16].The topography of the study area is extremely gentle with a few reliefs and surrounding ridges. Active and mobile sand dunes characterize its surface, which is probably because most of the northern, eastern, and southern boundaries of Al-Ahsa are located in the Al-Jafurah desert. The sand movement/drift originates from the northwest and north directions, estimated at 3 m^3/m width [15]. The sands surrounding the oasis are mobile in nature, and for numerous centuries, have been encroaching the cultivated land and endangering the oasis.

The areas around the Al-Ahsa municipality have arid and semi-arid climates. According to Mansour [17], the oasis is situated within a sub-tropic arid zone, which is characterized by extremely hot, dry summers and cool and relatively dry winter, with an average annual rainfall of almost less than 46 mm. According to Ait [15], the climate is arid; the mean temperature ranges from 26 to 27 °C and exceeds 45 °C during the summer season. The rainy season usually occurs in the winter months from December to April, whereas the highest mean amounts are found in January, March, and April of 18, 15.06, and 10.26 mm, respectively [15]. Economically, agriculture has been the major source of livelihood for the entire population. The agriculture in an oasis depends on the abundant water from the numerous springs and groundwater. It has been reported by Rahman et al. [13] that the Al-Ahsa area is an important and the largest agricultural area in the eastern region of Saudi Arabia. Furthermore, there are over 51 small towns scattered over the oasis, which is either fully or partially surrounded by date palms [14]. The oasis has more than 2 million palm trees, which produce thousands of tons of dates every year. Generally, the primary crops grown in the oasis are dates, wheat, barley, millet, rice, various fruits, vegetables, and alfalfa. The most important livestock raised are camels, sheep, goats, cattle, and donkeys [18]. Currently, the agricultural area is declining owing to climatic and anthropogenic factors, such as sand movement, urbanization encroachment, a decrease in the groundwater table level, and a lack of drainage (Sabakha) [15].

Data collection and pre-processing

The study work involved the use and analysis of two different types of satellite images to evaluate and analyse the response of selected VIs of different surface cover features over Al-Ahsa oasis, Eastern Region of Saudi Arabia. In this study, one scene (185 × 185 km) of Landsat 8 and another (290 × 290 km) of Sentinel-2A covering the study area (Figure 2) were selected and analyzed. The source, characteristics, and specifications of these two sensors are given in the following subsections.

Landsat 8 OLI

A Landsat 8 OLI accurate geometry [19], level 1 terrain-corrected (L1T) with narrow spectral bands, different spectral ranges, enhanced calibration, and a 12-bit radiometric resolution, was selected. It was acquired during the winter season, specifically on November 14 2017 (Table 1) from the United State Geological Survey (USGS), Global Visualization (GloVis) Data Bank, using the Worldwide Reference System (WRS) of path (ground-track-parallel) 164 and row (latitude-parallel) 42 coordinates [20].

Sentinel-2A MSI

Global Monitoring for Environment and Security (GMES) launched Sentinel-2A in a mission devoted to earth-observation purposes, in which essential elements of the space composed the system [21 - 23]. This mission provides continuous services utilizing multi-spectral high-spatial resolution (for optical regions) observations at global-terrestrial surface scales [24]. Further, the Sentinel-2A mission enables a unique combination of regular global land surface coverage, high revisit time of five days at the equator under same viewing situations, and wide-range field-of-view for multispectral observations from its 13 bands in the visible, near infra-red, and short wave infra-red regions. The sensor was designed to ensure operational supply of the data, providing e.g., hazard management (floods and forest fires and landslides), state and changes in the land use/land cover for Europe, forest monitoring, food security warning systems, water and soil management and protection, urban mapping, in addition to natural hazard prediction. The plan of the Sentinel-2A mission targets an operational multi-spectral earth-observation scheme that matches the Landsat and SPOT observations and enhances data obtainability for users.One Sentinel-2A image (10 m spatial resolution for optical bands) was downloaded from the USGS portal (https://earthexplorer.usgs.gov/) for November 14, 2017. The technical information for the two used sensors is provided in Table 1.

As stated by numerous researchers [4, 25 - 30], the use of satellite imagery with VIs needs various pre-processing techniques, such as radiometric and atmospheric corrections. These requirements are necessary to avoid misleading results that can be obtained from these issues. Accordingly, the OLI image was co-registered to Sentinel-2A with RMS <0.5. In addition, to compensate the atmospheric attenuation, two steps were performed. In the first step, all the spectral bands were converted from the digital number (DN) to the top-of-atmosphere reflectance, using the method described by Roy et al. [19]in the second step, dark object subtraction[31 – 33] was used to correct and minimize atmospheric effects, to analyse the surface reflectance of the different targets.

Table1; Characteristics and specifications of Landsat-8 OLI and Sentinel-2A data, obtained from USGS website.

Specifications of the Sensor	Sentinel-2A -T38QMH (Orbit No. 49)	Landsat-8 OLI
Path/row	164/42	164/42
Spectral bands	12 channels	11 channels
Acquisition date	November 14 2017	November 14 2017
Central wavelength (µm)*	Red (4) (0.665), infra-red (8) (0.842)	Red (4) (0.636-0.674), infra-red (5) (0.851-0.879)
Pixel (m)	10 m	30 m
Revisit frequency (days)	5	16

(*) Wavelength (µm) given only for the bands used in the SAVI and NDVI equations, which are red and infra-red channels.

To enhance the spatial resolution and visual interpretability of the surface features available with the Landsat-8 OLI bands, the Gram–Schmidt spectral pan-sharpening [32] and procedures described by Welch and Manfred Ehlers [34] were used to sharpen the low-spatial resolution band by employing a high-spatial resolution one. The resultant enhanced multispectral image had spatial resolution properties similar to those of the reference panchromatic band. This step was accomplished to approximate the resolution of the Landsat-8 image with those obtained from the Sentinel-2A bands for image to image comparisons. All these pre-processing steps were achieved by employing ENVI 5.3 and the QGIS Semi-Automatic plugin.

Data processing and analysis

Different spectral VIs have been developed to characterize and discriminate vegetation canopies [35] from other land cover materials. Red and near-infrared reflectance are the most common channels used by these indices. All these indices have been found to highly correlate with different vegetation factors (e.g., green leaf area, biomass, and photosynthetic activity) [36]. Herein, the most common (i.e., SAVI and NDVI) VIs were used, as detailed below.

SAVI

SAVI was developed by Huete [35] to minimize the soil brightness effect of spectral VIs using red and near-infrared (NIR) bands. The concept behind this index is to eliminate the soil-induced variation in VIs by adding a constant, L, to the NDVI Eq. The final Eq. of SAVI can be written as follows:

$$SAVI = \frac{(1+L)(\rho_{NIR} - \rho_{RED})}{\rho_{NIR} + \rho_{RED} + L} \quad (1)$$

Where the L value is a soil adjustment factor, varying between 0 and 1 according to the vegetation density. Optimization of the L factor would require prior knowledge of the vegetation amounts [37], and an optimal adjustment factor of 0.5 [35] for intermediate vegetation was found to reduce the soil background effects.

NDVI

The NDVI is a vegetation status indicator, which is intensively used for crop performance and health monitoring. The NDVI was calculated from the optical bands of the Sentinel-2A (MSI) and Landsat-8 (OLI) original and pan-sharpened pixels, i.e., the red (ρ_{RED}) and near-infrared (ρ_{NIR}) spectral bands for the acquired image. Specifically, Eq. (2) was applied38 using the ArcGIS software program.

$$NDVI = (\rho_{NIR} - \rho_{RED}) / (\rho_{NIR} + \rho_{RED}) \quad (2)$$

Linear correlation analysis

Spatial correlations have concrete importance in sub-pixel analysis because they assist in specifying a predictive relationship that can be exploited in accuracy enhancement of coarse-resolution satellite images. To realize the principal aim of this study, a process correlating three extracted spatial sets (Landsat (30-m based), Landsat (15-m based), and Sentinel (10-m based)) was performed. Sentinel-2A (10 m) was selected to represent the reference sensor for relative high-accuracy index extraction, since both sensors were selected due to their free availability, in addition to the high temporal frequency potentials. The acquired synchronous images were subjected to spectral sub-setting, in which ρRED and ρNIR were extracted to calculate the NDVI and SAVI over the area. Utilizing the tools of the ArcMap software program, a vectorization process was applied to the VI maps, so that pixels value in all the images were converted into points for tight correlation. A randomized selection of 100 base-points (earlier, pixels value) in the Landsat (30 m) raster-converted map was performed, and they were used as the principal extractors of the other VI values in all the other two sets (Landsat (15-m based), and Sentinel-2A (10-m based)), to be set in point forms. Hence, six (point-based) VI maps were extracted over

the study area and prepared for correlation, in which each NDVI, in addition to SAVI, was represented in the variant-scale sets (Landsat (30-m based), Landsat (15-m based), and Sentinel-2A (10-m based)).
The correlation relationships between the Sentinel-2A VIs and each of the variant-scale Landsat (30 m and 15 m) VIs were plotted at the base of the selected 100 points (Symmetrical positioning), producing four-type scatterplot representations, from which the impact of sensor spatial resolution on the quantification of the VIs could be addressed. Summarizing, the study hypothesized that for the high-spatial resolution images that were used for the VI extraction, high-feature separation accuracies in the image pixels were to be realized. Hence, Landsat (medium-scale resolution) informatics could still be enhanced by imposing the above correlation, utilizing the 10-m resolution of the Sentinel-2A images of the synchronous overpass times. Therefore, the pan-sharpened (15 m) Landsat VI maps were used to ensure that the possibility of enhancing the values of the extracted VIs corresponded to a 10-m resolution accuracy. The entire work procedure is shown in the flow chart in Figure 3, according to which the images of both the sensors are subjected to pre-processing, VI extraction, and vectorization, in addition to the correlation processes. All the processing steps were applied to the study area as well as to a selected cultivated area availed for validation.

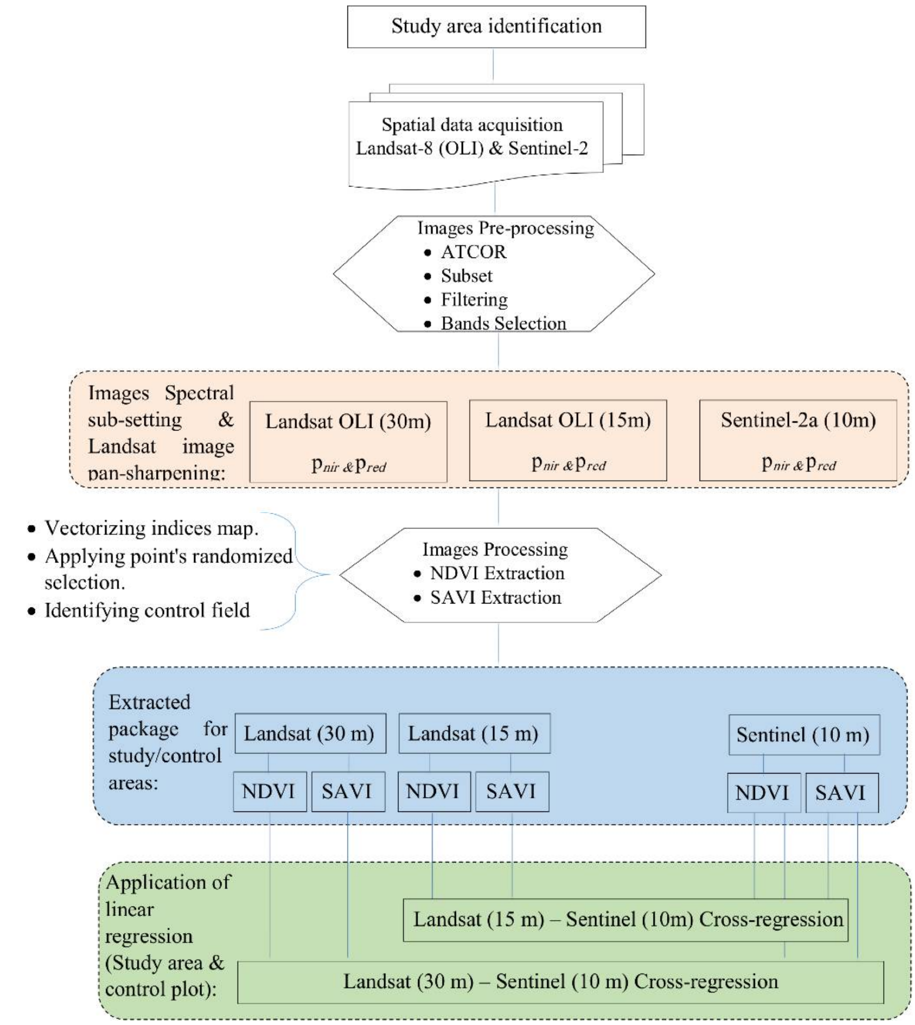

Figure3; Flow chart of the applied linear regression for the study area and the control plot.

Validation process

To examine the security, correctness, and relevance of the acquired VI sets of data, the study ran a validation process for the two differently acquired sensor VIs. A center-pivot scale irrigated field within the study area operated by NADA Dairy and Juices Company was selected to represent the control plot. The selected plot condition was a uniform surface covered with fully and homogeneously grown hay, used for grazing animals raised as livestock. Herein, the correlations between all the applied different-sized image pixels were assumed to be high. Thus, the produced correlation formulae were expected to be used for the enhancement of the Landsat coarse-pixel vegetation maps. For validation, a set of 60 VI points was extracted from the control plot.

RESULTS AND DISCUSSION

Measures of spatial distribution and variability

Data obtained in previous studies [2, 4, 38, 39], using different satellite images with different spatial resolutions, number of spectral bands, central wavelengths edges, and revisit times (e.g., MODIS, SPOT, AVHRR, Landsat (MSS, TM, ETM+, and OLI)) have indicated that the VIs calculated from these sensor systems are highly correlated to each other. Moreover, according to them, the improvements made with one sensor system can be used to predict the related information of other sensor systems. According to She et al. [2] and Steven et al. [39], the spectral ratio and NDVI, SAVI and EVI of the MSS, SPOT, and TM sensor systems were linearly correlated to those of the AVHRR system with an R^2 of approximately 0.9. The SAVI and NDVI results that were obtained from the Sentinel-2A and Landsat-8 images for this study are displayed in Figures. 4 and 5, respectively.

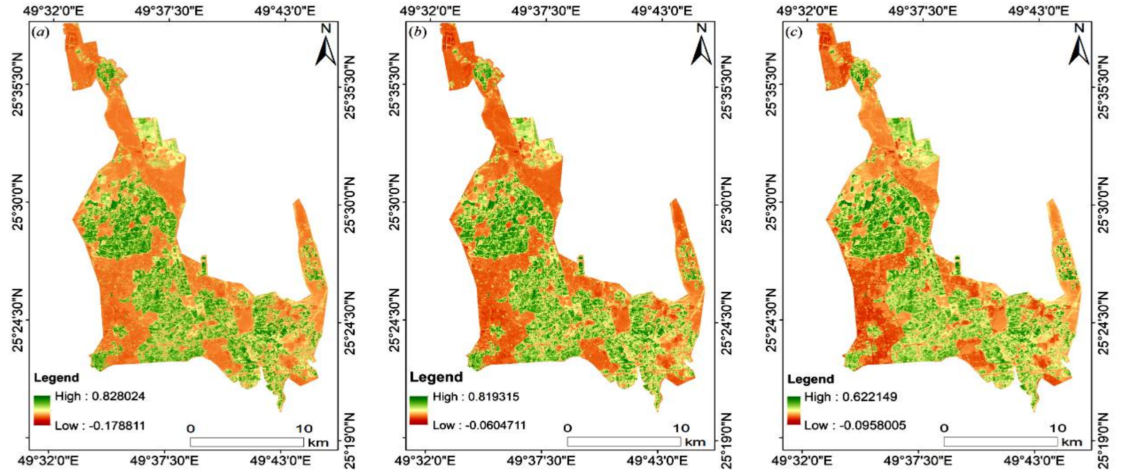

Figure4; The derived NDVI obtained from the calibrated Sentinel-2A and OLI satellite data: (a) show the NDVI values related to original OLI bands, (b) showing the NDVI values derived from the pan-sharpen channels. While (c) show the NDVI value calculated from the Sentinel-2A data.

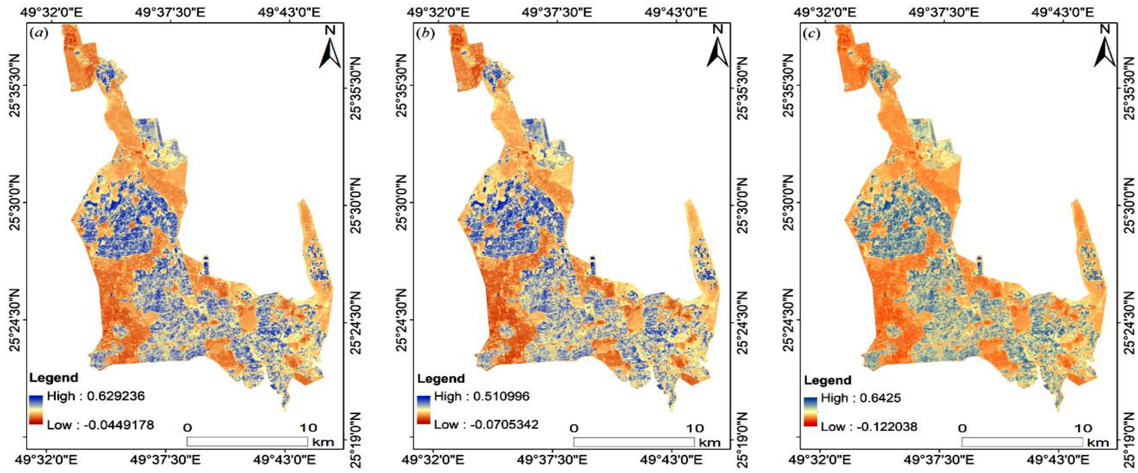

Figure5; The derived SAVI obtained from the calibrated Sentinel-2A and OLI satellite data using L = 0.5 to reduce soil background noise: (a) show the SAVI values related to original OLI bands, (b) showing the SAVL values derived from the pan-sharpen channels. While (c) show the SAVI value calculated from the Sentinel-2A data.

The statistical information related to each VI is provided in Table 2, where the arithmetic mean (μ), standard deviation (σ), and coefficient of variation (CV) are noticeably different for both the NDVI and SAVI of the two sensors. According to the standard deviation (σ), which is the positive square root of the variance [1], all the observations are noticeably closely clustered around a central value for both the SAVI and NDVI values. Comparing the standard deviation of the NDVI calculated from the original (OLI) bands to that from the pan-sharpened channels indicates that the values are scattered widely around the mean for the former than for the latter. Based on the CV, a relative measure of variation is detected between the derived VIs from the Sentinel-2A and OLI data. The NDVI and SAVI calculated from the OLI pan-sharpened bands have a large CV compared to those from the original bands.

Table2; Statistical information derived from the VIs obtained from both Sentinel-2A and OLI.

	Sentinel-2A					Landsat-8(OLI)				
	μ	σ	Min	Max	C.V	μ	σ	Min	Max	C.V
NDVI	0.21	0.16	-0.179	0.828	0.762	0.27, 0.13*	0.14, 0.08*	-0.060, -0.062*	0.662, 0.622*	0.518, 0.615*
SAVI	0.14	0.09	-0.122	0.642	0.643	0.19, 0.11*	0.08, 0.06*	-0.045, -0.045*	0.504, 0.511*	0.421, 0.545*

Note: * denotes the SAVI and NDVI statistical information calculated from pan-sharpened channels.

Among the different sensors, the CV of the VIs of Sentinel-2A is significantly higher than those for the VIs of the original and pan-sharpened channels. This indicates that there is an extremely high degree of skewness (clustered) to the right side of the mean with a low kurtosis (positively skewed), as is shown in the frequency distribution of the histograms in Figure 6. This suggests that most of the values of the two VIs are smaller than the mean. In fact, the positive skewness suggests the ascendancy of the green vegetation cover compared to the other land covers that are available in the study area. All the values in the histograms related to the VI are completely located in the positive scale edge, except the distribution of the histogram for the SAVI calculated from Sentinel-2A data, which entailed somewhat negative values. The above indicates that some of the SAVI values in the study area are larger than the mean. In addition, some pixels are completely covered by bare soil and pure sands, which have a larger visible reflectance than the near-infrared one. Furthermore, the variability of the vegetation cover in the study area is assessed to be less using the SAVI obtained from both the sensors, as exhibited by the measured standard deviations, whereas it i slightly higher using the NDVI. This finding suggests that using SAVI in areas dominated by date palm trees is more suitable for mapping, monitoring, evaluating, and assessing vegetation cover than using the NDVI. This result is in agreement with that of Alhammadi [40], who found out that in an area characterized by a complex land cover and dominated by date palm trees, the SAVI was a highly suitable method to detect the vegetation health. However, the mean, standard deviation, coefficient of variation, skewness, and kurtosis only provide a basic assessment of different distributions, and cannot measure the correlation, response, and continuity of the VIs from the two used sensors.

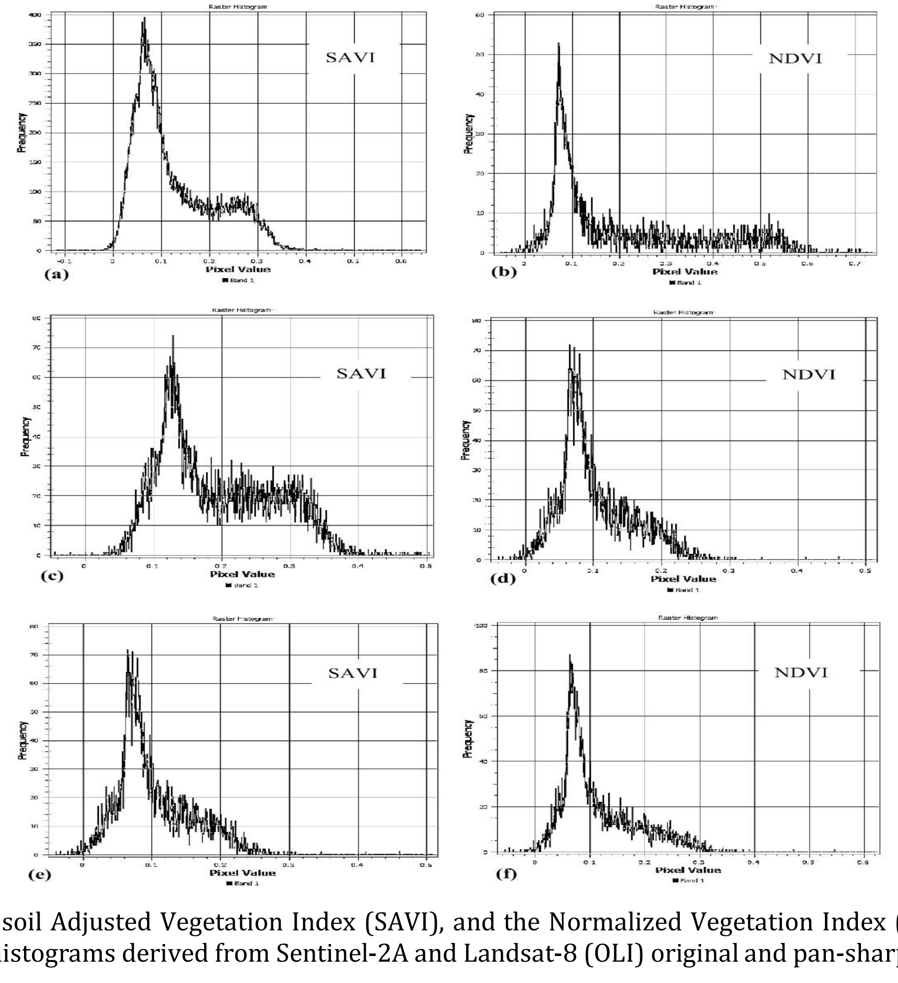

Figure 6;The soil Adjusted Vegetation Index (SAVI), and the Normalized Vegetation Index (NDVI) pixels distribution histograms derived from Sentinel-2A and Landsat-8 (OLI) original and pan-sharpen channels.

Evaluation of resultant areas covered by green vegetation

To evaluate the sensitivity of the VIs obtained from the different sensors (i.e., Sentinel-2A, original, and resized-pixel OLI), the area covered by vegetation was calculated and is listed (in squared-kilometer and percentage) in Table 3. As can be seen, there are considerable and noticeable differences (4.32 %, 4.54%) between Sentinel-2A and original-pixel OLI for SAVI and the NDVI, respectively, whereas subtle differences (0.39%, 0.4%) are found for the original and pan-sharpened OLI, with the values being almost identical. The obtained results exhibit that the spatial resolution has a significant effect on the accuracy of the land use/cover mapping and assessment. This is particularly for an area such as the Al-Ahsa oasis, which is dominated by date palm trees, with a mixture of different surface cover types existing beneath the palm canopies. Although this information was obtained from datasets subjected to precise calibration and atmospheric effect corrections, some difference might have arisen owing to the variation in the band wavelength widths of the three sets, as provided in Table 1. However, the obtained results were not consistent with those of Cicvo [41], who documented that the topography effect had a major impact on the radiance received by the ground cover targets and sensors simultaneously. Sometimes the variation in the SAVI and NDVI values can be attributed to soil conditions, as displayed by a study conducted recently by Allbed et al. [12], who revealed that a reduction in the NDVI values could be measured in areas affected by salinization, similar to certain parts in the Al-Ahsa oasis. The same study [12] revealed that as the salinity rate changes, the vegetation cover changes, particularly in an area dominated by date palm trees. In addition to the above studies, Huete [35] documented that in areas surrounded by a soil of high brightness (e.g., sand dunes), the VI values will be affected by the variations resulting from different soil factors, particularly roughness variations. The observed differences in the maximum values of the NDVI and SAVI might be explained by the soil-adjustment factor (L = 0.5) value related to SAVI. This value reduces the effect of the soil background, which has a significant impact; however, it was not considered in the NDVI calculation. The theoretical basis of this effect could be described by the following explanation: "vegetated canopy will scatter and transmit a significant amount of NIR flux toward the soil surface, irradiating the soil underneath as well as in between individual plants. The soil subsequently reflects part of this scattered and transmitted flux back toward the sensor, in a manner dependent on the optical properties of the soil surface" [35]. Previously, Dawelbait and Morari [42] confirmed that under areas having arid and semi-arid conditions, the NDVI had a limitation in providing accurate estimates of the vegetation cover owing to the spectral variability of background materials such as the soil spectral albedo. This caused a non-linearity in the correlation between the NDVI and vegetation physical characteristics and between the different sensor systems.

Table3; Illustration of the area covered by green vegetation using SAVI and the NDVI for Sentinel-2A, original, and pan-sharpened Landsat-8 (OLI) images.

Sensors	Sentinel-2A	Original-OLI	Pan-sharpened-OLI	Differences (%)
VIs	The area in (km^2)			
SAVI	92.833 (35.54%)	104.094(39.86%)	103.343(39.57%)	4.32% - 0.39%
NDVI	83.589(32.00%)	95.419(36.54%)	96.469(36.94%)	4.54% - 0.4%

Correlation analysis result (consistency and reliability of VIs)

Numerous studies [2, 4, 5, 19, 20, 27, 38, 39, 43 – 45] have proven that there is a linear relationship between the VIs derived from coarse, moderate, and high-spatial resolution sensor systems (e.g., MODIS, AVHRR, MSS, TM, ETM+, SPOT). In this study, to examine the consistency between the VIs derived from the different calibrated sensor systems (i.e., Sentinel-2A MSI and Landsat-8 OLI original and pan-sharpened), a correlation analysis was performed by using 100 samples collected from the Sentinel-2A MSI as the dependent variables, and those from the Landsat-8 original and resized/pan-sharpened-OLI as independent variables. However, there was no noticeable distinction between the dependent and independent variables; the correlation was only a measure of the association of two variables, as in Clark & Hosking [46]. The resultant linear plots of the relationships are presented in Figure 7. For SAVI, the scatterplots of both the original-pixel OLI and resized-pixel OLI versus Sentinel-2A are remarkably identical, with an R^2 of 0.76 for both. However, for the NDVI, the correlation between the original-pixel OLI and Sentinel-2A is found to be weak, with an R^2 of 0.50, compared to when Sentinel-2A is correlated to the pan-sharpened-pixel OLI (R^2 = 0.76). This significant weak correlation can be explained by the subtle differences between the central wavelengths (spectral resolution) of the two sensor systems, specifically the red band and near-infrared band edges, as documented in Table 1. In addition, there is a difference in the spatial resolution, as reported in previous literatures [32, 42], according to which, the 30-m pixel size may contain mixed features with different reflectance values (as explained in the background section). These mixed features may influence the final value of the NDVI, as documented by

Unger Holtz [1], who stated that 'the greater the amount of healthy green vegetation in the instantaneous field of view (IFOV) of the sensor, the greater the NDVI value'. Simultaneously, the good correlation between SAVI of the Sentinel-2A and pan-sharpened-pixel OLI is most likely owing to the proximity between the pixel sizes that was accomplished after pan-sharpening. Hence, the spatial proximity was observed to be an influencing factor because of the spectral similarity in the consistencies of the sensors. Gallo and Daughtry [43] found a high correlation between the AVHRR and MSS, and indicated that the AVHRR data could estimate the VIs of the MSS owing to the similarity in the bandwidths of the two sensor systems. Furthermore, the findings of this study also confirm a study conducted recently by Zhang et al. [5], who documented a high correlation between the Sentinel-2A MSI and Landsat-8 OLI, with an $R^2 >$ 0.87, 0.89, and 0.90 for atmospherically corrected data. They concluded that the consistency between the Sentinel-2A MSI and Landsat-8 OLI data can be improved by ordinary least-squares (OLS) linear regression.

It was revealed from the relatively good correlation between the SAVIs obtained from the Sentinel-2A MSI and original Landsat-8 OLI, the sensitivity of SAVI was higher for arid and semi-arid ecosystems, in which the predominant cover type is date palm. Consequently, the progress achieved with the Sentinel-2A sensor might be applied to estimate and predict the Landsat-8 OLI system using the slopes and intercepts of Sentinel-2A, as documented by Gallo and Daughtry [43].

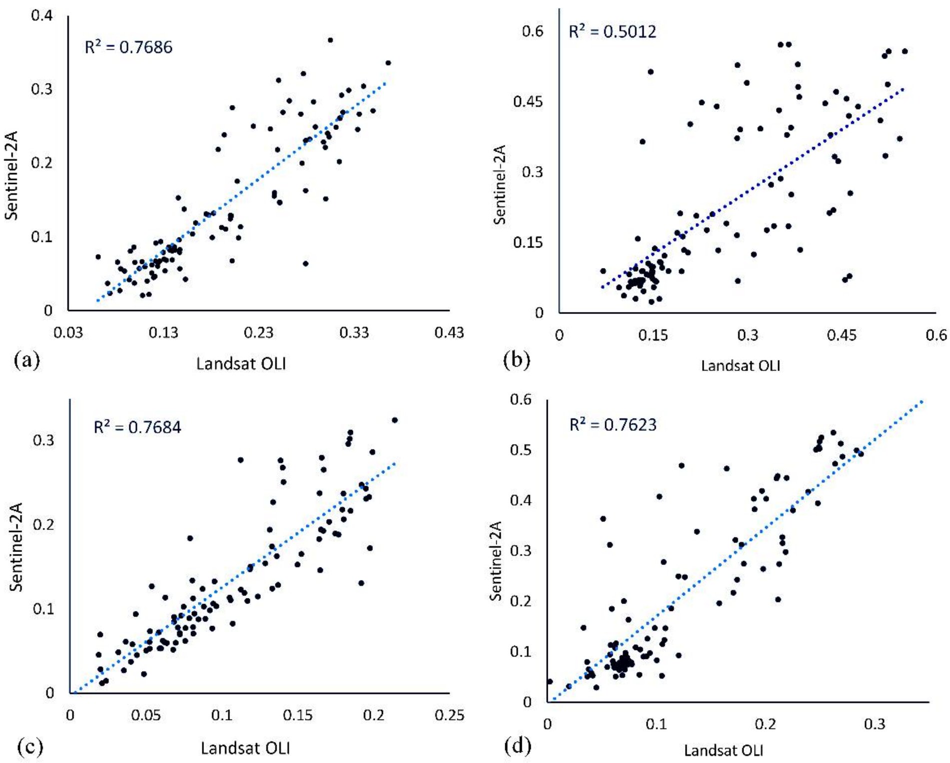

Figure7;The scatterplot shows the correlation among vegetation indices (a) SAVI and (b) NDVI, derived using Sentinel-2A (Y-axis) and original OLI (X-axis); and (c) SAVI and (d) NDVI, derived using Sentinel-2A (Y-axis) and OLI (pan-sharpened-15 m). All the VIs were calculated based on TOA reflectance data, where a total of 100 random samples were collected from each image and then analyzed for correlation using the Coefficient of Determination (r^2).

Validation of continuity of VI derived from Sentinel-2A and Landsat-8 OLI

To confirm the study results, the validation process for the VIs obtained from the two different sensors was performed using a uniform and homogenous irrigated field allocated within the study area. A set of 60 VI sample points were collected from the uniformly grown vegetation. The scatter plot representations given in Figure 8 (a and b) shows the resultant validations of the extracted Sentinel–Landsat NDVI and SAVI, respectively, over the cultivated plot. The correlations yield an R^2 of 0.60 and 0.61 for the NDVI and SAVI, respectively. Remarkably, the weak nature of the relationships can be noticed, particularly when compared to the directly applied correlations over the study area. Although the study considered the vegetation cover homogeneity, similarity in all the atmospheric and weather conditions, and synchronous sensor overpass times, there is a noticeable variation in the VIs. This can be mainly attributed to the difference in the spectral regions for the bands that are used for assessing the VIs, as provided in Table 1.

This variability in the optimized VIs supports numerous similar findings in previous research studies [43], in which the differences in the satellite-based sensor systems, in addition to their waveband differences, can be the reasons for the VI variation.

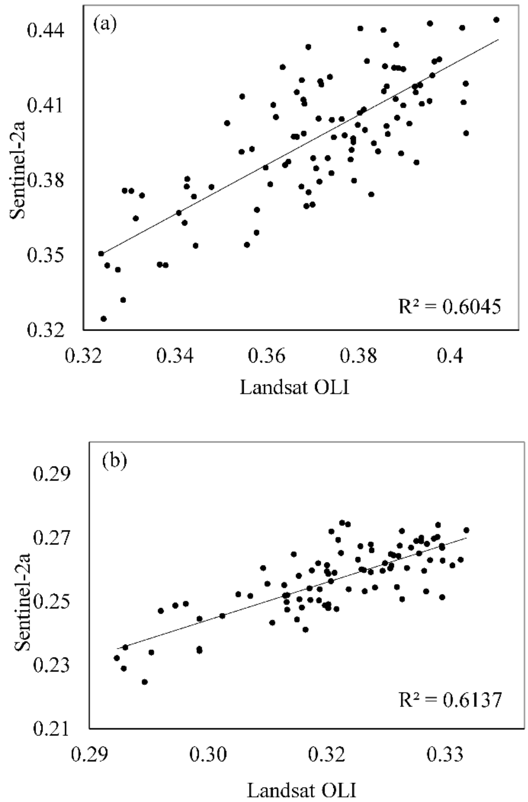

Figure8;Scatterplots of the (a) NDVI and (b) SAVI, for the two sensors (Sentiel-2A and Original-OLI), in which a set of 60 VI points was extracted from the control plot for validation purpose.

Owing to the rapid effect of some applied nitrogen (N) fertilizers on cultivated crops (control plot), there is a noticeable difference in the agronomic variables of a canopy, as stated by Gallo and Daughtry [43]. This also supports and explains the weakness of applying VI control plots for different sensors. The acquired validation also confirms a study by Zhang et al. [5], where the ranges of the MSI and OLI values indicate a considerable spectral variation in terms of the measuring surface type and conditions for winter and summer months, across a specific study area. Zhang et al. [5] in his recently conducted study, justified it by the existent of many confounding reasons, including spectral band pass differences, with a probability of other factors involvement; such as atmospheric contamination, bi-directional reflectance differences and calibration.

CONCLUSION

Assessing the quantitative variation in the VIs derived from the freely available resources of the Landsat-8 OLI and Sentinel-2A MSI, was the focal aim of this study to confirm the findings of earlier research. These were reported and confirmed the spatial dissimilarity in surface objects due to the differences in the specifications of sensors. Consequently, these differences have become critical issues in the application of remotely sensed data to vegetation monitoring and assessment. This study employed OLI (30 m), OLI pan-sharpened (15 m), and MSI (10 m) data for multi-surface cover features dominated mostly with date palm, to examine their consistency and reliability in the extraction of the VIs, in the forms of the NDVI and SAVI.

The statistics related to the derived VI showed noticeable differences in both the NDVI and SAVI of the three spatial datasets, according to which the VI variability was less when using the SAVI for both the sensors, as revealed by the standard deviations. In comparison, it was slightly higher when using the NDVI. This finding suggested that the use of SAVI in the areas dominated by date palm trees was more suitable for the mapping, monitoring, evaluation, and assessment of vegetation cover than using the NDVI. Further, to evaluate the sensitivity of the VIs of the different sensors, the area covered by the vegetation was calculated and assessed to have noticeable differences (4.32 %, 4.54 %) in SAVI and the NDVI, respectively, for Sentinel-2A and original-pixel of OLI. Furthermore, subtle differences (0.39 %, 0.40 %) were found between the original and pan-sharpened-pixel OLI images for SAVI and the NDVI, respectively. These results indicated that the spatial resolution had a significant effect on the land use/cover mapping accuracy. Furthermore, the applied correlation between the variant-scale-extracted VIs revealed moderate agreements for SAVI producing R^2 of 0.76 between the Sentinel-2A and both the original-pixel Landsat OLI, as well as the pan-sharpened-pixel Landsat OLI. In comparison, there was a weak correlation in the NDVIs acquired from the original-pixel OLI and Sentinel-2A MSI with an R^2 of 0.50. This could be attributed to the differences in the spectral and spatial resolutions of the two sensors, in addition to the insensitivity of the NDVI in considering the effect of the soil background beneath the palm canopies. Finally, the validation process that was conducted at the uniformly cultivated field to obtain the VIs using the two different sensors yielded weak correlations when compared to the directly applied ones over the study area, producing an R^2 of 0.60 for both the NDVI and SAVI. This could also be mainly owing to differences in the spectral regions for the bands that were used for the VI assessment. Further research is needed to study other factors that lead to different results when using different images, such as sand dunes and topographic effects.

REFERENCES

1. Unger HTS. (2007). Introductory Digital Image Processing: A Remote Sensing Perspective, Third Edition. Environmental and Engineering Geoscience; 13(1): 89–90.
2. She X, Lifu Z, Yi C, Taixia W, Changping H, Muhammad HAB. (2015). Comparison of the Continuity of Vegetation Indices Derived from Landsat 8 OLI and Landsat 7 ETM+ Data among Different Vegetation Types. Remote Sensing; 7(10): 13485–506.
3. Schmugge TJ, William PK, Jerry CR, Thomas JJ, Rango Al. (2002). Remote Sensing in Hydrology. Adv Water Resour.; 25(8): 1367–85.
4. Hill J, Dorothea A. (1990). Comparative Analysis of Landsat-5 TM and SPOT HRV-1 Data for Use in Multiple Sensor Approaches. Remote Sens Environ; 34(1): 55–70.
5. Zhang HK, David PR, Lin Y, Zhongbin L, Haiyan H, Eric V, Sergii S, Jean-claude R. (2018). Remote Sensing of Environment Characterization of Sentinel-2A and Landsat-8 Top of Atmosphere , Surface , and Nadir BRDF Adjusted Re Fl Ectance and NDVI Di Ff Erences. Remote Sens Environ; 215(April): 482–94.
6. Song Y, Ma M, Veroustraete F. (2010). Comparison and conversion of AVHRR GIMMS and SPOT Vegetation NDVI data in China. Int J Remote Sens.; 31(9): 2377–92.
7. Aldakheel YY. (2011). Assessing NDVI Spatial Pattern as Related to Irrigation and Soil Salinity Management in Al-Hassa Oasis, Saudi Arabia. Journal of the Indian Society of Remote Sensing; 39(2): 171–80.
8. Elprince A, Makkp YM, Ai-Barrak S, Tamim MT. (1982). Use of computer graphics in developing density maps for the date culture of Al-hasa oasis in saudi arabia. In Proceedings of the First Symposium on Date Palm, King Faisal University, AI-Hassa, Saudi Arabia.
9. Abdelatti H, Elhadary Y, Babiker AA. (2017). Nature and Trend of Urban Growth in Saudi Arabia : The Case of Al-Ahsa Province – Eastern Region. Resour Environ.; 7 (3): 69–80.
10. Roberts DA, Philip D, Susan U, Ernie R, Marco M. (1999). Development of a Regionally Specific Library for The Santa Monica Mountains Using High Resolution Aviris Data. Accessed December 31, 2018.
11. Statistics GA. (2010). Population and Housing Atlas, Maps Distributions of Preliminary Results. Hofuf. https://www.stats.gov.sa/sites/default/files/en-dmaps2010_0_0.pdf.
12. Allbed A, Kumar L, Sinha P. (2018). Soil Salinity and Vegetation Cover Change Detection from Multi-Temporal Remotely Sensed Imagery in Al Hassa Oasis in Saudi Arabia. Geocarto International; Vol (33) Taylor & Francis.
13. Abdul-Rahman, Alghannam O, Alhajhoj MR, Al-Qahtnai. (2012). Impact of Vegetation Cover on Urban and Rural Areas of Arid Climates. AJAE; Vol 3.
14. Alqarni S, Abbas B, Salih A. (2018). Detection, Mapping and Assessment Change in Urban and Croplands Area in Al-Hassa Oasis, Eastern Region in Saudi Arabia Using Remote Sensing and Geographic Information System. Journal of Geographic Information System; 10(06): 659–85.
15. Ait M. (2019). TS8 Geographic Information for Planning Urban-Rural Land Use Change Detection and Analysis Using GIS & RS Technologies. https://www.fig.net/resources /proceedings/fig_proceedings/ morocco/ proceedings /TS8/TS8_1_belaid.pdf.
16. Elhadary YA, Al-Omair AA. (2014). Indicators and Causes of Rural Settlement Changes in Saudi Arabia: Alhasa Province in the Eastern District as Case Study. Journal of the Gulf and Arabian Peninsula Studies. Gulf and Arabian Peninsula Studies; 40(155).
17. Mansour A. (1984). The Development of the Eastern Province, with Particular Reference to Urban Settlement and Evolution in Eastern Saudi Arabia. http://etheses.dur.ac.uk.
18. Abderrahman W. (1988). Water Management Plan for the Al-Hassa Irrigation and Drainage Project in Saudi Arabia. Agricultural Water Management; 13(2–4): 185–94.
19. Roy DP, Kovalskyy V, Zhang HK, Vermote EF, Yan L, Kumar SS, Egorov A. (2016). Characterization of Landsat-7 to Landsat-8 Reflective Wavelength and Normalized Difference Vegetation Index Continuity. Remote Sens Environ.; 185: 57–70.

20. Ke Y, Jungho I, Junghee L, Huili G, Youngryel R. (2015). Characteristics of Landsat 8 OLI-Derived NDVI by Comparison with Multiple Satellite Sensors and in-Situ Observations. Remote Sens Environ.; 164: 298–313.
21. Bertini F, Brand O, Carlier S, Umberto DB, Matthias D, Duca R, Fernandez V, et al. (2012). Sentinel-2 ESA's Optical High-Resolution Mission for GMES Operational Services. ESA Bulletin. Bulletin ASE. European Space Agency; SP-1322.
22. Donlon C, Berruti B, Buongiorno A, Ferreira MH, Féménias P, Frerick J, Goryl P, et al. (2012). The Global Monitoring for Environment and Security (GMES) Sentinel-3 Mission. Remote Sens Environ.; 120(May): 37–57.
23. Torres R, Paul S, Dirk G, David B, Malcolm D, Evert A, Pierre P, et al. (2012). GMES Sentinel-1 Mission. Remote Sens Environ.; 120(May): 9–24.
24. Martimort P, Olivier A, Michael B, Roberto B, Bernardo C, Umberto DB, Valérie F, et al. (2007). Sentinel-2 Optical High Resolution Mission for GMES Operational Services. In International Geoscience and Remote Sensing Symposium (IGARSS); 2677–80.
25. Bao N, Alex ML, Andrew F, Andrew M, David M, Zhongke B. (2012). Comparison of Relative Radiometric Normalization Methods Using Pseudo-Invariant Features for Change Detection Studies in Rural and Urban Landscapes. Journal of Applied Remote Sensing; 6 (1): 063578-1.
26. Chander G, Brian L M, Dennis L H. (2009). Summary of Current Radiometric Calibration Coefficients for Landsat MSS, TM, ETM+, and EO-1 ALI Sensors. Remote Sens Environ.; 113(5): 893–903.
27. Price JC. (1987). Calibration of Satellite Radiometers and the Comparison of Vegetation Indices. Remote Sens Environ.; 21(1): 15–27.
28. Sinha P, Lalit K. (2013). Independent Two-Step Thresholding of Binary Images in Inter-Annual Land Cover Change/No-Change Identification. ISPRS J Photogramm Remote Sens.; 81: 31–43.
29. Yang X, Lo CP. (2000). Relative Radiometric Normalization Performance for Change Detection from Multi-Date Satellite Images. Photogrammetric Engineering and Remote Sensing.; 66(8): 967–80.
30. Yuan D, Christopher DE. (1996). Comparison of Relative Radiometric Normalization Techniques. ISPRS J Photogramm Remote Sens.; 51(3): 117–26.
31. Alqurashi AF, Kumar L. (2017). An Assessment of the Impact of Urbanization and Land Use Changes in the Fast-Growing Cities of Saudi Arabia. Geocarto International; 6049: 1–20.
32. Research Systems. (2004). ENVI User's Guide, September, 1–1150. https://doi.org/10.1111/ j.16000447 .2011.01711.x.
33. Song C, Curtis EW, Karen CS, Mary PL, Scott AM. (2001). Classification and Change Detection Using Landsat TM Data. Remote Sens Environ.; 75(2): 230–44.
34. Welch R, Manfred E. (1987). Merging Multi-resolution SPOT HRV and Landsat TM Data. Photogrammetric Engineering and Remote Sensing.; 53(3): 301.
35. Huete AR. (1988). A Soil-Adjusted Vegetation Index (SAVI). Remote Sens Environ.; 25(1): 295–309.
36. Tucker CJ. (1979). Red and Photographic Infrared Linear Combinations for Monitoring Vegetation. Remote Sens Environ.; 8(2): 127–50.
37. Qi J, Chehbouni A, Huete AR, Kerr YH, Sorooshian S. (1994). A Modified Adjusted Vegetation Index (MSAVI). Remote Sens Environ.; 48(2): 119–26.
38. Ritchie JC, Charles MC, Frank RS. (1990). The Relationship of MSS and TM Digital Data with Suspended Sediments, Chlorophyll, and Temperature in Moon Lake, Mississippi. Remote Sens Environ.; 33(2): 137–48.
39. Steven MD, Timothy JM, Frédéric B, Hui X, Mark JC. (2003). Intercalibration of Vegetation Indices from Different Sensor Systems. Remote Sens Environ.; 88(4): 412–22.
40. Alhammadi MS, Glenn EP. (2008). Detecting Date Palm Trees Health and Vegetation Greenness Change on the Eastern Coast of the United Arab Emirates Using SAVI. Int J Remote Sens.; 29(6): 1745–65.
41. Cicvo D. (1989). Topographic Normalization of Landsat Thematic Mapper Digital Imagery. Photogrammetric Engineering and Remote Sensing; 55: 1303–9.
42. Dawelbait M, Morari dF. (2012). Monitoring Desertification in a Savannah Region in Sudan Using Landsat Images and Spectral Mixture Analysis. J Arid Environ.; 80: 45–55.
43. Gallo KP, Daughtry CST. (1987). Differences in Vegetation Indices for Simulated Landsat-5 MSS and TM, NOAA-9 AVHRR, and SPOT-1 Sensor Systems. Remote Sens Environ.; 23(3): 439–52.
44. Song Y, Mingguo M, Frank V. (2008). Comparison and Conversion of AVHRR GIMMS and SPOT Vegetation NDVI Data in China. Int J Remote Sens.; 31(9): 2377–92.
45. Yin H, Thomas U, Rasmus F, Dirk P, Patrick H. (2012). How Normalized Difference Vegetation Index (NDVI) Trends from Advanced Very High Resolution Radiometer (AVHRR) and Système Probatoire d'observation de La Terre Vegetation (SPOT VGT) Time Series Differ in Agricultural Areas: An Inner Mongolian Case Study. Remote Sensing; 4(11): 3364–89.
46. Clark WAV, Hosking PL. (1986). Statistical Methods for Geographers. Wiley; https://doi.org/10.1016/ j.enconman.2010.10.037.